Numerical investigation of poroelastic effects during hydraulic fracturing using XFEM combined with cohesive zone model

Xiaoyu Ren [1], Yueyang Guan [2], Xiaofei Zhang [3], Xiaobao Liu [3], Jie Liu [3], Kang Liu [4], Jiangwei Luo [5], Guiyuan Shi [5]

[1] The Second Gas Production Plant of Petro China Changqing Oilfield Company, Yulin, China
[2] CNPC Engineering Technology R&D Company Limited, Beijing, China
[3] The Second Gas Production Plant of Petro China Changqing Oilfield Company, Yulin, China
[4] CNPC Bohai Drilling Engineering Company Limited No.4 Drilling Engineering Company, China
[5] China University of Petroleum (Beijing), China

Abstract. Hydraulic fracturing is an effective technology used to stimulate hydrocarbon production from unconventional reservoirs. Numerical simulation of the hydraulic fracturing process plays a key role in the design of hydraulic fracturing. However, most of existing models are overly simplified by neglecting the poroelasticity of rock matrix, which may have a substantial effect on the growth of hydraulic fractures, especially in oil and/or water saturated formations. In this study, we developed a fully coupled finite element model for hydraulic fracture propagation in permeable formations by combining XFEM technique with cohesive zone model, and used it to investigate the effects of poroelasticity on the geometry evolution of single fracture which initiated from an injection point. Fluid flow within the fractures, Darcy flow within the rock matrix, hydraulic fractures propagation, and fluid leak-off into the formation are simultaneously taking into account in the model. Then, the model is validated by comparing the results with available analytical solutions. To understand and quantify the poroelastic effects on the propagation of hydraulic fracture, several cases with different matrix permeability, leak-off coefficients, and bulk modulus of pore fluid are performed. The simulation results show that the total volume of leakage is controlled by the combined action of matrix permeability and leak-off coefficient. The fracture aperture and length decrease with the increase of matrix permeability or leak-off coefficient, while as the bulk moduli of pore fluid increases, the fracture aperture and length tend to increase.

Keywords: Poroelastic effect; Hydraulic fracturing; XFEM; Cohesive zone model.

1. Introduction

Hydraulic fracturing is an effective technology used to stimulate hydrocarbon production from unconventional reservoirs, in which one or more fractures are driven by the internal pressurized fluid (Bunger and Cardella, 2015). The growth of hydraulic fracture in porous media is a complex, multi-physics problem, which can be generally considered as the following coupled processes (Adachi et al., 2007; Detournay, 2016): (i) rock deformation caused by the fluid pressure on the fracture surfaces, (ii) fluid flow within the fracture, (iii) fracture propagation, and (iv) fluid leak out of the fracture into the formation matrix. Accurately predicting the growth behavior of hydraulic fracture is necessary to design a suitable fracturing scheme, which requires a fully coupled numerical model that can simultaneous account for the aforementioned processes.
In the early times, analytical and semi-analytical methods (Detournay, 2004; Nordgren, 1972; Perkins and Kern, 1961) have been developed to understand the evolution of

variables of interests, such as fracture aperture, fracture length, and injection pressure. Due to the inherent limitation of analytical methods, these solutions, however, are usually limited to some simple situations such as constant injection rate and linearly elastic medium. To simulate the growth behavior of hydraulic fracture in more sophisticated situations, a large number of numerical approaches have been proposed in literatures, including the boundary element method (Gordeliy and Detournay, 2011; Long and Xu, 2017; Zhang and Jeffrey, 2008), the distinct element method (Damjanac and Cundall, 2016; Han et al., 2015), the finite element method (Carrier and Granet, 2012; Guo et al., 2015; Li et al., 2017a; Li et al., 2017b), the finite discrete element method (FDEM) (Lisjak et al., 2017; Yan et al., 2015), the discontinuous deformation method (DDA) (Choo et al., 2016), and the extended finite element method (XFEM) (Mohammadnejad and Khoei, 2013; Salimzadeh and Khalili, 2015). Although significant progress has been made, there are still some critical points that need to be elucidated. For example, most of existing models use

Carter leak-off model to characterize the velocity of fluid leak out of fracture, but neglect the poroelasticity effect of rock matrix, which may have substantial impacts on the growth of hydraulic fracture, especially in oil and/or water saturated formations.

To understand and quantify the poroelasticity effect on the evolution of hydraulic fracture, this paper develops a fully coupled XFEM-based cohesive model which is able to take into account several crucial physical aspects during hydraulic fracture propagation in porous media, including fracture propagation, fluid flow within fracture, fluid leak-off, pore fluid flow, and rock deformation. In the following, the governing equations used in the model are provided first. Next, this model is validated against analytical solutions. Finally, parametric sensitivity analyses are performed to investigate the impact of poroelastic effect on the growth of hydraulic fracture.

2. Governing equations

2.1 Deformation of porous medium

The rock formation is assumed to be a homogeneous, isotropic, and linear poroelastic medium. For quasi-static conditions, the stress equilibrium equation can be written as

$$\nabla \cdot \boldsymbol{\sigma} + \mathbf{F} = 0 \tag{1}$$

where $\mathbf{F}$ is the body force vector, and $\boldsymbol{\sigma}$ is the total stress tensor. Assuming that the rock matrix is fully saturated by single-phase fluid and obeys poroelasticity theory, the effective stress of rock matrix reads (Detournay and Cheng, 1993)

$$\boldsymbol{\sigma}' = \boldsymbol{\sigma} + \alpha p \mathbf{I} \tag{2}$$

where $\boldsymbol{\sigma}'$ is the effective stress, p is the pore pressure, $\mathbf{I}$ is the second-order unit matrix, and α is the Biot coefficient, which is defined as

$$\alpha = 1 - K / K_s \tag{3}$$

where K and K_s are the bulk modulus of porous rock and of the rock matrix grain, respectively. The effective stress is related to the matrix strain as

$$\boldsymbol{\sigma}' = \mathbf{D}\boldsymbol{\varepsilon} \tag{4}$$

where $\mathbf{D}$ is the elastic stiffness matrix, and $\boldsymbol{\varepsilon}$ is the strain tensor.

The pore fluid flow obeys mass balance equation as

$$\frac{\partial \left(\rho_f \phi \right)}{\partial t} + \nabla \cdot \left(\rho_f \phi \mathbf{v}_f \right) = 0 \tag{5}$$

where ρ_f is pore fluid density, ϕ is the rock porosity, $\mathbf{v}_f$ is the fluid flow velocity of the pore fluid. The Darcy's fluid velocity is given by

$$\mathbf{v}_d = \phi \left(\mathbf{v}_f - \mathbf{v}_s \right) \tag{6}$$

in which $\mathbf{v}_s$ is the solid phase (rock matrix) velocity, and $\mathbf{v}_d$ is the Darcy's fluid velocity, can be defined as

$$\mathbf{v}_d = \frac{\mathbf{k}_m}{\mu_f} \left(\nabla p + \rho_f \mathbf{g} \right) \tag{7}$$

in which $\mathbf{k}_m$ is the permeability of the rock matrix, μ_f is the fluid viscosity, and $\mathbf{g}$ is the vector of gravitational acceleration.

2.2 Fracture fluid flow

Assuming that the hydraulic fracture is filled with a Newtonian fluid, the mass balance equation for the fluid flow within the fracture reads (Hibbitt et al., 2016)

$$\dot{w} + \nabla \cdot q + \left(q_t + q_b \right) = 0 \tag{8}$$

where w is the fracture width, q is the tangential fluid flow velocity within the fracture, q_t and q_b are the fluid leak-off into the formation across top and bottom fracture surfaces, respectively.

The tangential fluid flow velocity obeys cubic law as

$$q = -\frac{w^3}{12\mu_f} \nabla p_f \tag{9}$$

in which p_f is the fluid pressure within the fracture.

The normal fluid velocity per unit area (q_t and q_b) can be described as

$$\begin{cases} q_t = c_t \left(p_f - p_t \right) \\ q_b = c_b \left(p_f - p_b \right) \end{cases} \tag{10}$$

where p_t and p_b are the pore fluid pressures in the rock matrix abut to the top and bottom surfaces, respectively. c_t and c_b are the "leak-off coefficients" of top and bottom surfaces, respectively. Different with the classical Carter's model, c_t and c_b here characterize the resistance of fluid across the fracture surfaces. The leak-off velocity is controlled by the rock matrix permeability if c_t and c_b are large enough.

2.3 Fracture propagation

XFEM technique, implemented in Abaqus, is used in this paper to simulate the hydraulic fracture propagation in porous media. The fracture propagation behavior is described by cohesive zone model with linear traction-separation response, as shown in Fig. 1. Damage is assumed to initiate when a quadratic interaction function involving nominal stress ratios reaches 1.0, which can be expressed as (Hibbitt et al., 2016)

$$\left(\frac{\langle t_n \rangle}{t_n^0} \right)^2 + \left(\frac{t_s}{t_s^0} \right)^2 + \left(\frac{t_t}{t_t^0} \right)^2 = 1 \tag{11}$$

where t_n, t_s, and t_t are the nominal traction in the normal and two local shear directions, respectively; t_n^0, t_s^0, and t_t^0 represent the cohesive strength in the normal and two local shear directions, respectively.
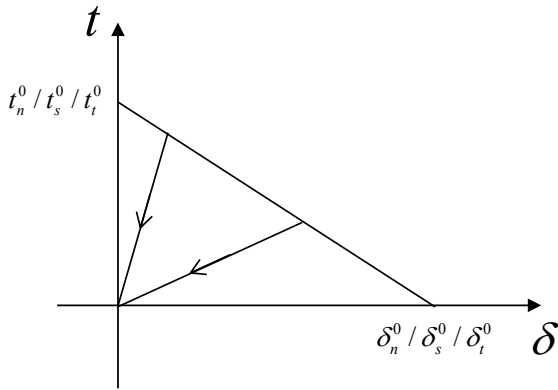
Fig. 1 Linear elastic traction-separation law

Damage evolution of cohesive zone model is described by progressive degradation of cohesive strength as

$$t_0 = \begin{cases} (1-D)T_n & T_n \geq 0 \\ T_n & T_n < 0 \end{cases} \quad (12)$$

$$t_{s/t} = (1-D)T_{s/t} \quad (13)$$

where $T_{n/s/t}$ are the stresses in the corresponding directions predicted by linear traction-separation law without damage. D is the scalar damage parameter.

3. Model validation

In this section, Terzaghi's problem and KGD problem are performed to verify the capability of the XFEM-based cohesive zone model on modeling the process of fluid diffusion and the growth of hydraulic fracture in rock matrix, respectively.

3.1 Terzaghi's problem

Consider a water-saturated, plane strain porous column, with the height of 100 m, as shown in .Fig. 2(a). The top surface is drained and other surfaces are undrained boundary conditions. The normal displacement of left, right, and bottom boundaries are fixed. A load P_L acts instantaneously on the top boundary at initial time. The relevant parameters of this case are shown in Table. 1 and the analytical solution are provided in Appendix A.

Table. 1 Input parameters for the Terzaghi's problem

Parameters	Value
Elastic moduli, GPa	1.0
Poisson's ratio	0.0
Bulk moduli of grain, GPa	50.0
Bulk moduli of pore fluid, GPa	2.2
Permeability, D	1.0
Fluid viscosity, mPa·s	1.0
Load P_L, MPa	1.0

Fig. 2(b) shows the evolution of pore pressure along the length of the column at different time, and Fig. 2(c) shows the vertical displacement of top boundary. The numerical results agree well with analytical solutions, which

indicates that the XFEM-based cohesive model has the capability to model the fluid diffusion of rock matrix.
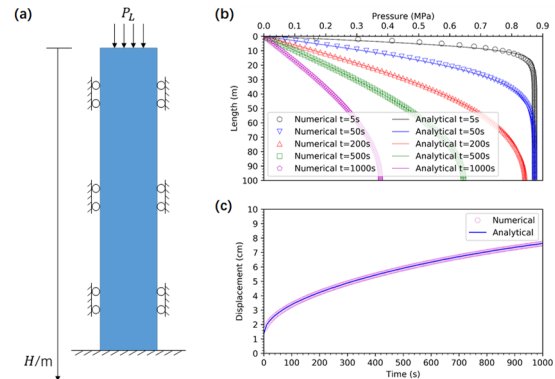

Fig. 2 (a) Sketch of the Terzaghi's problem; (b) Evolution of pore pressure along the length of the column; (c) Vertical displacement of top boundary

3.2 KGD problem

As shown in Fig. 3(a), a bi-wing fracture is created by injecting a Newtonian fluid into an impermeable medium. Because the typical growth of hydraulic fracture in an unconventional reservoir is under viscosity dominated, the parameters used in this case were tuned to this regime, as provided in Table. 2. The details of semi-analytical solutions are shown in Appendix B.

Fig. 3 (b) and (c) show the temporal evolution of injection pressure and mouth aperture. The agreement between numerical results and analytical solutions is very good, which proves the adequacy of the XFEM-based cohesive zone model on modeling the growth of hydraulic fracture.

Table. 2 Input parameters for the KGD problem

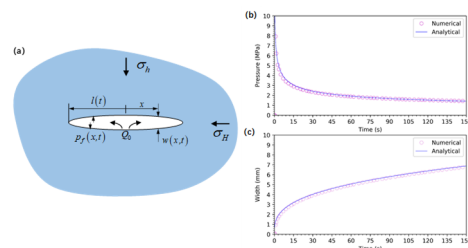| Parameters	Value
Elastic moduli, GPa	10.0
Poisson's ratio	0.2
Mode-I fracture energy, J/m²	10
Mode-II fracture energy, J/m²	300
Tensile cohesive strength, MPa	0.2
Shear cohesive strength, MPa	0.2
Injection rate, m³/s	5×10^{-4}
Fluid viscosity, Pa·s	2.0
Injection time, s	150.0

Fig. 3 (a) Sketch of the KGD problem; (b) Temporal evolution of injection pressure; (c) Temporal evolution of mouth aperture

4. Poroelastic effect on hydraulic fracture propagation

This section aims to investigate the impact of poroelastic effect on the propagation behavior of hydraulic fracture. To this end, a series of parametric analyses for KGD problem are performed in this section. As shown in Fig. 4, a 2D plane-strain fracture is propagated by injecting a viscos fluid from the initial crack. The dimension of the domain is 200×50 m, and the length of the initial crack is 0.4 m. The left boundary of the model is symmetric boundary condition, the normal displacements of other external boundaries are fixed, and a constant pore pressure boundary condition is also imposed on these boundaries. The input parameters for the base case of parametric analysis are listed in Table. 3. Additionally, in each parametric analysis, only the investigated parameter is changed while all other parameters are kept same with the values from the base case.

Table. 3 Input parameters for the base case

| Parameters	Value
Elastic moduli, GPa	20.0
Poisson's ratio	0.2
Mode-I fracture energy, J/m^2	10
Mode-II fracture energy, J/m^2	300
Tensile cohesive strength, MPa	0.2
Shear cohesive strength, MPa	0.2
Permeability, D	1.0
Leak-off coefficient, m/(Pa·s)	$1.0×10^{-5}$
Bulk moduli of pore fluid, GPa	2.2
Initial pore pressure, MPa	20.0
$\sigma_H/\sigma_h/\sigma_v$, MPa	30/27/35
Fluid viscosity, Pa·s	0.1
Injection rate, m^3/s	$5×10^{-4}$
Injection time, s	80.0
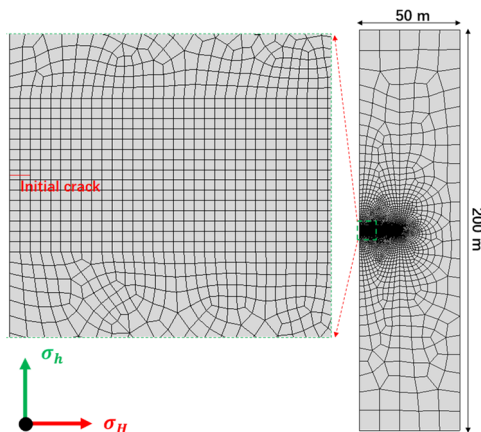
Fig. 4 The geometry and mesh of the KGD problem

4.1 Results of the base case

Fig. 5 shows the final fracture geometry and pore pressure distribution of the base case. The fracture grows to a length of 6.2 m at the end of the simulation (t=80 s). The leak-off coefficient in this case is large enough and the rock permeability dominates the fluid leak velocity. The simulation results for temporal evolution of net injection pressure and aperture at the injection point are shown in Fig. 6. The maximum aperture at the end of simulation is about 1.35 mm.
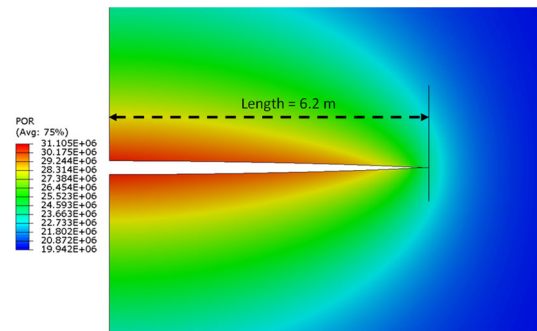

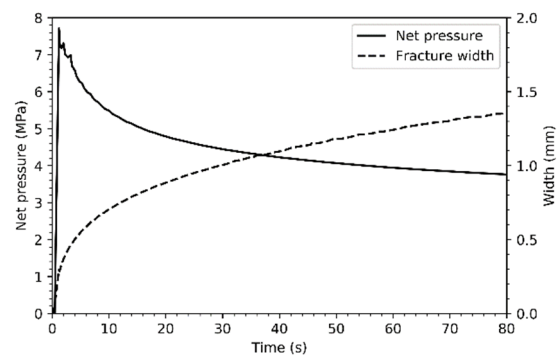Fig. 5 Fracture geometry and pore pressure distribution of the base case at the end of the simulation

Fig. 6 Temporal evolution of net injection pressure and aperture at the injection point

4.2 Effect of permeability

As an important parameter for porous media properties, permeability is expected to significantly influence the pore pressure distribution around the hydraulic fracture, and consequently affects the fracture evolution. Thus, we perform a sensitivity analysis by varying permeability in this section. Assume there is no filter cake developed on the fracture surfaces. Fig. 7 depicts the fracture profile and pore pressure distribution at the end of the injection for different rock permeability. It readily observed that fracture length increases monotonically as permeability decreases. Large permeability leads to high fluid loss volume, which indicates that the leak-off in a system with large leak-off coefficient is controlled by rock permeability.
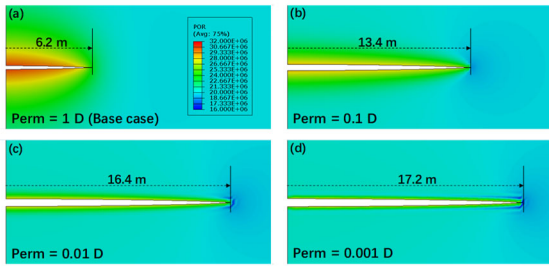
Fig. 7 Effect of permeability on the fracture profile and pore pressure distribution

Fig. 8 shows the effect of permeability on the net pressure and aperture at the injection point as time elapse. It can be observed that the net pressure of high permeability case is much larger than the low permeability case, while the fracture aperture of high permeability case is much lower than the low permeability case. This is due to the large back-stress induced by poroelastic effect in high permeability case, which in turn reduces the aperture.
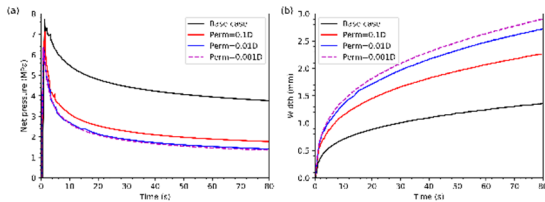

Fig. 8 Effect of permeability on the net pressure and aperture at the injection point

4.3 Effect of leak-off coefficient

Leak-off coefficient in this work characterizes the resistance of filter-cake during the fracture propagation. Fig. 9 shows that the impact of leak-off coefficient on the growth of hydraulic fracture is substantial. Fluid loss is controlled by permeability in base case while it is controlled by the leak-off coefficient in Fig. 9(d) and consequently more fluid is utilized to drive the fracture propagation.
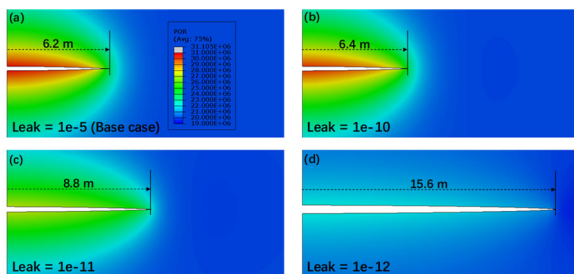

Fig. 9 Effect of leak-off coefficient on the fracture profile and pore pressure

Fig. 10 shows the temporal evolution of net pressure and aperture at the injection point for different leak-off coefficient. The results indicate that lower leak-off coefficient results in lower propagation pressure and higher fracture aperture. This is because the back-stress induced by poroelastic effect is lower.
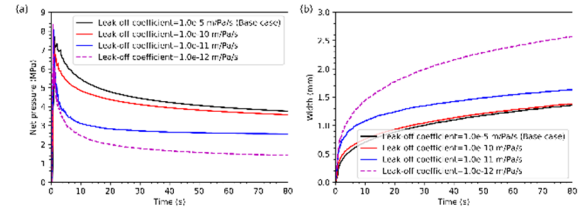

Fig. 10 Effect of Leak-off coefficient on the net pressure and aperture at the injection point

4.4 Effect of bulk modulus of pore fluid

Bulk moduli of pore fluid is one of factors determining the dissipation rate of pore pressure, which may influence the hydraulic fracture propagation. However, to the authors' knowledge, there is no previous studies have investigated its influence on the fracture propagation. Fig. 11 shows the fracture profiles for different bulk modulus of pore fluid. The results indicate that low bulk moduli of pore fluid tends to suppress the increase of the pore pressure around hydraulic fracture, which leads to high leak-off velocity and low fracturing fluid efficiency.
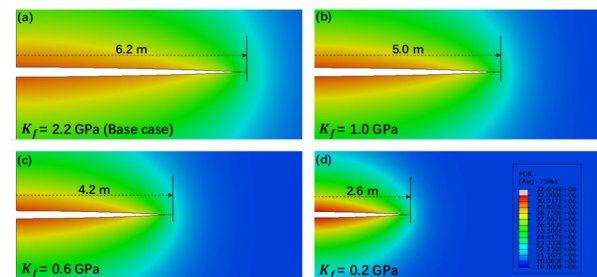

Fig. 11 Effect of fluid bulk moduli on the fracture profile and pore pressure

5. Conclusions

In this paper, a fully coupled finite element model is proposed to investigate the influences of poroelastic effect on the growth of hydraulic fracture, and the model was validated against available solutions. The simulation results show that the total volume of leakage is controlled by the combined action of matrix permeability and leak-off coefficient. The fracture aperture and length decrease with the increase of matrix permeability or leak-off coefficient, while as the bulk moduli of pore fluid increases, the fracture aperture and length tend to increase.

Acknowledgements

Appendix A. Terzaghi's 1D consolidation problem(Wang, 2004)

Pore pressure evolution:

$$p(z,t) = \frac{4}{\pi} p_0 \sum_{m=0}^{\infty} \frac{1}{2m+1} \exp\left[\frac{-(2m+1)^2 \pi^2 ct}{4L^2}\right] \sin\left[\frac{(2m+1)\pi z}{2L}\right] \quad \text{(A.1)}$$

Vertical displacement:

$$u(z,t) = c_M p_0 \left\{ (L-z) - \frac{8L}{\pi^2} \sum_{m=0}^{\infty} \frac{1}{(2m+1)^2} \exp\left[\frac{-(2m+1)^2 \pi^2 ct}{4L^2}\right] \cos\left[\frac{(2m+1)\pi z}{2L}\right] \right\} + u_0 \quad \text{(A.2)}$$

where $p_0(z) = \frac{\alpha M}{K_u + 4\mu/3} P_L$; $u_0(z) = \frac{1}{K_u + 4\mu/3} P_L(L-z)$;

$M = \left[\phi\beta + (\alpha - \phi)c_{br}\right]^{-1}$ is the Biot modulus; c_{br} is the solid grain compressibility; K_u is the undrained bulk modulus; c_M is the vertical uniaxial compressibility; c is the consolidation coefficient.

Appendix B. Viscosity dominated KGD problem

A bi-wing fracture is created by injecting an incompressible Newtonian fluid into rock. The rock is assumed to be impermeable and under a plane strain condition. The fluid injection rate is Q_0. Fracture half-length $l(t)$, fracture aperture $w(x,t)$, and net pressure of the fracture $p(x,t)$ will be determined, where x is the distance along the fracture and t is injection time. The analytical solutions of this problem are provided by Detourney (Detournay, 2004) as functions of the injection rate Q_0 and three material parameters E', K', and μ',

$$E' = \frac{E}{1-v^2}; \quad K' = 4\left(\frac{2}{\pi}\right)^{1/2} K_{IC}; \quad \mu' = 12\mu; \quad \text{(B.1)}$$

where K_{IC} is the fracture toughness, E is the Young modulus, v is the Poisson ratio, and μ is the fluid viscosity.

The solutions provided by Detourney (Detournay, 2004) can be expressed as:

$$l(t) = L(t)\gamma(t); \quad w(x,t) = \varepsilon(t)l(t)\Omega(\xi,t);$$
$$p(x,t) = \varepsilon(t)E'\Pi(\xi,t) \quad \text{(B.2)}$$

where $\xi = x/l(t)$ is the scaled coordinate $(0 \le \xi \le 1)$; $\varepsilon(t)$ is a small dimensionless parameter; $L(t)$ is length scale; γ, Ω, and Π are dimensionless fracture length, aperture, and net pressure, respectively.

In viscosity-dominated propagation regime, the aforementioned dimensionless parameters can be expressed as follows:

$$\varepsilon(t) = \left(\frac{\mu'}{E't}\right)^{1/3}; \quad L(t) = \left(\frac{E'Q_0^3}{\mu'}\right)^{1/6} t^{2/3} \quad \text{(B.3)}$$

$$\gamma_{m0} = 0.616 \quad \text{(B.4)}$$

$$\bar{\Omega}_{m0}(\xi) = A_0\left(1-\xi^2\right)^{2/3} + A_1^{(1)}\left(1-\xi^2\right)^{5/8} + B^{(1)}\left[4\sqrt{1-\xi^2} + 2\xi^2 ln\frac{1-\sqrt{1-\xi^2}}{1+\sqrt{1-\xi^2}}\right] \quad \text{(B.5)}$$

$$\Pi_{m0} = \frac{1}{3\pi} B\left(\frac{1}{2},\frac{2}{3}\right)\left[A_{02}F_1\left(-\frac{1}{6},1;\frac{1}{2};\xi^2\right) + \frac{10}{7}A^{(1)}{}_2F_1\left(-\frac{7}{6},1;\frac{1}{2};\xi^2\right)\right] + B^{(1)}(2-\pi|\xi|) \quad \text{(B.6)}$$

where $A_0 = 3^{1/2}$; $A_1^{(1)} = -0.156$; $B^{(1)} = 0.0663$; B is the Euler beta function; and $_2F_1$ is a hypergeometric function.

References

1. Adachi, J., Siebrits, E., Peirce, A. and Desroches, J., 2007. Computer simulation of hydraulic fractures. International Journal of Rock Mechanics and Mining Sciences, 44(5): 739-757.

2. Bunger, A.P. and Cardella, D.J., 2015. Spatial distribution of production in a Marcellus Shale well: Evidence for hydraulic fracture stress interaction. Journal of Petroleum Science and Engineering, 133: 162-166.

3. Carrier, B. and Granet, S., 2012. Numerical modeling of hydraulic fracture problem in permeable medium using cohesive zone model. Engineering Fracture Mechanics, 79: 312-328.

4. Choo, L.Q., Zhao, Z., Chen, H. and Tian, Q., 2016. Hydraulic fracturing modeling using the discontinuous deformation analysis (DDA) method. Computers and Geotechnics, 76: 12-22.

5. Damjanac, B. and Cundall, P., 2016. Application of distinct element methods to simulation of hydraulic fracturing in naturally fractured reservoirs. Computers and Geotechnics, 71: 283-294.

6. Detournay, E., 2004. Propagation regimes of fluid-driven fractures in impermeable rocks. International Journal of Geomechanics, 4(1): 35-45.

7. Detournay, E., 2016. Mechanics of Hydraulic Fractures. Annual Review of Fluid Mechanics, 48: 311-339.

8. Detournay, E. and Cheng, A.H.-D., 1993. Fundamentals of poroelasticity, Chapter 5 in Comprehensive Rock Engineering: Principles, Practice and Projects, II, pp. 113-171.

9. Gordeliy, E. and Detournay, E., 2011. Displacement discontinuity method for modeling axisymmetric cracks in an elastic half-space. International Journal of Solids and Structures, 48(19): 2614-2629.

10. Guo, J., Lu, Q., Zhu, H., Wang, Y. and Ma, L., 2015. Perforating cluster space optimization method of horizontal well multi-stage fracturing in extremely thick unconventional gas reservoir. Journal of Natural Gas Science and Engineering, 26: 1648-1662.

11. Han, Y., Hampton, J., Li, G., Warpinski, N.R. and Mayerhofer, M.J., 2015. Investigation of Hydromechanical Mechanisms in Microseismicity Generation in Natural Fractures Induced by Hydraulic Fracturing. SPE Journal.

12. Hibbitt, H., Karlsson, B. and Sorensen, P., 2016. Abaqus Analysis User's Manual Version 2016, Dassault Systèmes Simulia Corp, Providence.

13. Li, Y. et al., 2017a. Numerical simulation of limited-entry multi-cluster fracturing in horizontal well. Journal of Petroleum Science and Engineering, 152: 443-455.

14. Li, Y., Deng, J.G., Liu, W. and Feng, Y., 2017b. Modeling hydraulic fracture propagation using cohesive zone model equipped with frictional contact capability. Computers and Geotechnics, 91: 58-70.

15. Lisjak, A. et al., 2017. A 2D, fully-coupled, hydro-mechanical, FDEM formulation for modelling fracturing processes in discontinuous, porous rock masses. Computers and Geotechnics, 81: 1-18.

16. Long, G. and Xu, G., 2017. The Effects of Perforation Erosion on Practical Hydraulic-Fracturing Applications. SPE Journal, 22(02): 645 - 659.

17. Mohammadnejad, T. and Khoei, A.R., 2013. An extended finite element method for hydraulic fracture propagation in deformable porous media with the cohesive crack model. Finite Elements in Analysis and Design, 73: 77-95.

18. Nordgren, R., 1972. Propagation of a vertical hydraulic fracture. Society of Petroleum Engineers Journal, 12(04): 306-314.

19. Perkins, T. and Kern, L., 1961. Widths of hydraulic fractures. Journal of Petroleum Technology, 13(09): 937-949.

20. Salimzadeh, S. and Khalili, N., 2015. Fully coupled XFEM model for flow and deformation in fractured porous media with explicit fracture flow. International Journal of Geomechanics, 16(4): 04015091.

21. Wang, H.F., 2004. Theory of linear poroelasticity with applications to geomechanics and hydrogeology.

22. Yan, C., Zheng, H., Sun, G. and Ge, X., 2015. Combined Finite-Discrete Element Method for Simulation of Hydraulic Fracturing. Rock Mechanics and Rock Engineering, 49(4): 1-22.

23. Zhang, X. and Jeffrey, R.G., 2008. Reinitiation or termination of fluid-driven fractures at frictional bedding interfaces. Journal of Geophysical Research: Solid Earth, 113(B8).